A method to account for transient performance requirements in the design of steam generators for concentrated solar power applications

Ferruzza, Davide; Kærn, Martin Ryhl; Haglind, Fredrik

Published in:
Applied Energy

Link to article, DOI:
10.1016/j.apenergy.2020.114931

Publication date:
2020

Document Version
Peer reviewed version

A method to account for transient performance requirements in the design of steam generators for concentrated solar power applications

Davide Ferruzza[a], Martin Ryhl Kærn[a], Fredrik Haglind[a]

[a]*Department of Mechanical Engineering, Technical University of Denmark, 2800 Kongens Lyngby, Denmark*

Abstract

Concentrating solar power plants are strongly characterized by recurring start-up and shut-down procedures. This imposes new challenges for conventional components such as the steam generator systems, as frequent load variations might lead to high thermal stress cycles, affecting their lifetime negatively. In this context, the header and coil design is a favourable configuration to reduce stresses. This paper introduces a method to design the heat exchangers of the header and coil steam generator type accounting for the dynamic performance, thermal stress sensitivity and impact on the performance of the power plant. Optimal designs were determined by minimizing the cost and total water-side pressure drop of the steam generator and the levelized cost of electricity of the power plant. The steam generator dynamic model was successfully validated using operational data. The results suggest that a steam generator design characterized by a tube outer diameter of 30 mm, high steam generator pressure drop and low investment cost is the optimal solution for the power plant under consideration. A configuration featuring a large number of tube layers is optimal in order to reduce the pressure drop at the superheater while at the same time, guaranteeing acceptable stresses and good transient response.

Keywords: Concentrating solar power, Parabolic trough power plants, Steam generator, Start-up, Thermal stresses, Dynamic performance

Nomenclature

Abbreviations

ACC air cooled condenser

BPVC boiler pressure vessel code

C controller

CSP concentrating solar power

CT cold tank

D deaerator

ECO economizer

EVA evaporator

FW feedwater

HP high pressure

HT hot tank

IHX indirect heat exchanger

IRE integral relative error

LP low pressure

NRMSE normalized root mean squared error

PID proportional integral derivative

PTPP parabolic trough power plant

PV process variable

RH re-heater

RMSE root mean squared error

SF solar field

SGS steam generator system

SH superheater

SM solar multiple

ST steam Turbine

TEMA tubular exchanger manufacturers association

TES thermal energy storage

UTS ultimate tensile strength

Subscripts

b bend

e parallel to the economizer

f frictional

i inside

l liquid

M mechanical

m metal

o outside

s parallel to the superheater

T thermal

t total

v vapor

Symbols

α	stress concentration factor,	[-]
β	thermal expansion coefficient,	$[K^{-1}]$
$\dot{m}$	mass flow rate,	[kg/s]
$\dot{Q}$	heat rate,	[W]
λ	thermal conductivity,	$[W/(mK)]$
ν	Poisson ratio,	[-]
ω	wetted perimeter,	$[m^2]$

ρ	density,	[kg/m^3]
σ	stress,	[Pa]
θ	tube coil angle of bend,	[rad]
φ	specific heat,	[W/kg]
A	area,	[m^2]
C_f	Fanning friction factor,	[−]
c_p	specific heat at constant pressure,	[kJ/(kg K)]
$CAPEX$	capital expenditure,	[USD]
CRF	capital recovery factor,	[-]
f_{D}	Darcy's friction factor,	[-]
g	Earth's gravitational constant,	[m/s^2]
h	enthalpy / heat transfer coefficient,	[J/kg] / [W/(m^2 K)]
h	specific enthalpy,	[J/kg]
i	real interest rate,	[-]
ID	internal diameter,	[m]
k	bend loss coefficient,	[-]
k_{i}	annual insurance rate,	[-]
L	length,	[m]
$OPEX$	operational expenditure,	[USD/year]
p	pressure,	[bar]
r	radius,	[m]
T	temperature,	[°C]
u	internal energy,	[J/kg]

V	volume,	[m^3]
v	velocity,	[m/s]
x	spatial coordinate,	[m]
z	vertical coordinate,	[m]
E	Young's modulus,	[Pa]
U	overall heat transfer coefficient,	[$W/(m^2K)$]

1. Introduction

Concentrating solar power (CSP) plants are an attractive renewable energy technology due to their key characteristic of being flexible towards the electricity production. The capability to integrate relatively cheap thermal energy storage (TES) systems allows the plants to decouple the solar input from the electricity production, enabling them to play a key role in the fluctuating electricity grid loads [1]. Moreover, the use of TES allows for the integration of a high capacity of intermittent renewable energy, thus making CSP constituting a key role in the energy transition [2]. Though being a promising solution, CSP plants are not competitive yet with the more traditional fossil fuel based power plants. From a technical standpoint, the inherent stochastic and cyclic nature of the solar radiation induces frequent changes in load and necessitates regular start-up and shut-down procedures in the absence of high capacity TES. Improving the operating performance and flexibility of its components towards cyclic loads is a way to overcome these challenges and improve the performance of the power plants. In this way, it is possible to increase the electric energy yield and profitability by utilizing the solar irradiation as quickly and as effectively as possible [3]. However, in order to guarantee the desired lifetime of some components, the maximum gradient of temperature (heating rate) is generally constrained by thermo-mechanical limitations.

Parabolic trough power plants are the most mature technology both from an economic and a technical perspective. They make up around 80 % of both the planned to be constructed and existing power plants [4–6]. Additionally, parabolic trough systems not only attract interest in the power sector, but also in other thermal applications, such as water desalination [7]. In these power plants, the traditional fossil fuel boiler is substituted by a series of parabolic mirrors to concentrate the direct solar irradiation onto the receiver tubes

and convert the solar energy into high temperature heat. The heat is converted to electricity with a Rankine cycle. The connection between the power block (PB) and the solar field (SF) is the steam generator system (SGS). It is characterized by a train of heat exchangers which transfer the useful heat from a heat transfer fluid (HTF) to the liquid water coming from the feedwater (FW) system of the Rankine cycle. The water temperature is increased until reaching the required superheated steam conditions for the inlet of the turbine [5].

The SGS and the steam turbine are generally the components which pose the main constraints with regards to the rate of the power block start-up [8]. The high thermo-mechanical stresses on the thick-walled component junctions impose a limitation on the maximum heating rates at which the steam generator can experience a water temperature increase [9–11]. The main constraint usually derives from the evaporator steam drum, which is designed as a high diameter pressure vessel, therefore consisting of thick walls. The maximum allowable heating rates are determined following the European norm (EN) 12952-3 [12], according to low-cycle fatigue requirements. The start-up procedure of the component is intended to reach nominal conditions for mass flow rates as fast as possible, and pressure and temperature.

Considering the steam turbine, the shaft thickness poses limitations to the start-up procedure rapidness of the component. The starting temperature of the metal determines the appropriate start-up schedule curve that needs to be selected to minimize the temperature difference between the metal and the steam. The selected start-up curve defines the synchronization delay and the time for the turbine to reach full load (or ramp delay). During the synchronization phase, the pressure is kept constant and the turbine is rolled-up to the nominal speed with a low mass flow rate. During the ramp delay phase, the pressure and mass flow rate are increased to the turbine nominal load [13, 14]. Therefore, when considering the start-up of the SGS, the turbine constraints need to be taken into account as they impose a boundary condition on the heat exchangers.

Many operating CSP plants were integrated with SGSs which were designed conventionally (i.e. for baseload application) and therefore not suited for dynamic conditions [15]. The header and coil design is one of the available configurations that overcomes such problems. Avoiding thick flat plates as in the TEMA (Tubular exchanger manufacturers association) cases [16], with the employment of circular manifolds, allows for lower thermo-mechanical stress [17]. For a more comprehensive description of the header and coil geometry, the reader is referred to Ref. [18]. Such design has recently gained traction and interest in the industry. It was installed in the first commercial Indian CSP plant (parabolic trough) and in the

Shenzen Jinfan molten salt solar tower power plant[19].

There is a rising number of works dealing with the analysis of the steam generator systems. These are applied to numerous fields, not only related to renewable power generation, as many of the previous works on steam generator systems are dedicated to nuclear power applications. For instance, Chen et al. [20] and Liu et al. [21] analysed a natural circulation evaporator for pressurized water reactors by employing optimization algorithms. More recently, due to the need to overcome the fossil fuel dependency in the energy field, the interest in SGS technologies was not only aimed towards CSP technologies, but also other renewable energy forms. For instance, Mercati et al. [22] developed a method to design a SGS for a system which produced both hydrogen and superheated steam. On the CSP side, Gomez-Hernandez et al. [23] performed an exergonomic analysis in order to design SGSs for solar tower power plants. In addition, Lin et al. [24] described a design routine for direct steam generation solar tower power plants. The dynamics of steam generators in CSP plants was also investigated in the past [25], the work did not provide appropriate design requirements for such components.

The thermal design of the heat exchangers is mainly defined by two main steps: the estimation of heat transfer area and related pressure drops, and the assessment of the cost. The minimization of the cost and the pressure drop are conflicting, and the steps can be coupled to determine optimal trade-off curves. There are many methods available in literature, to determine the required heat transfer area of heat exchangers [26–28], but considering tube banks and slightly complex geometries, the method summarized by Anarratore et al. [29, 30] can be applied to modify the logarithmic mean temperature based on the tube configurations. This can be coupled with cost estimation functions [31] to determine the overall investment costs. In literature several works can be found regarding the application of such methods to the design of heat exchangers and SGS systems [32–34]. Gonzalez-Gomez et al. [16] developed a cost-based optimization method to find the trade-off between the SGS cost and the power plant levelized cost of electricity (LCOE). In these studies, the dynamic performance was not analysed or taken into account during the design stage of the heat exchangers and SGSs. Nonetheless, when considering power plants experiencing highly dynamic operating conditions as in the CSP case, the dynamic performance may become of vital importance for the remunerative aspects of the power plant.

These points led to increased interest in the analysis of the dynamic performance, and this is to some extent revealed in literature. The dynamic performance of the SGSs was investigated both for parabolic trough power plants [35] and solar tower power plants [36].

In another research work, Mertens et al. [37] compared the transient response during a fast start-up procedure between a once-through and a natural circulation steam generator. Additionally, Gonzalez-Gomez analyzed the lifetime of the components of the SGS for a solar tower power plant application according to the ASME norms [38]. The authors did not consider impact on power plant performance or the influence of the lifetime estimation on the redesign of the steam generator system. In the context of the specific configurations of the heat exchangers, Pelagotti et al. [17] and Gonzalez-Gomez et al. [39] evaluated the thermal stress evolution of the header and coil design and more conventional TEMA designs, respectively, in order to analyze if the stresses were within the allowable limits; however, these thermal stress evaluations were not part of the SGS design optimization.

In a previous work [18], we presented a method to account for the low-cycle fatigue constraints during the design phase of the heat exchangers according to the EN 12952-3. The geometry was optimized by minimizing the total water-side pressure drop and investment costs, considering minimum values for maximum allowable heating rate, determined based on the annual performance of the power plant. However, we did not consider the transient performances of the heat exchangers and their impact on the performance of the PTPP. As an outcome of the work optimal SGS designs minimizing the cost and water pressure drop were presented. However, this work focused on the component design only and did not include any considerations of the influence of the SGS design on the power plant performance. Additionally, the work presented by Gonzalez-Gomez et al. [35] proved that the CSP SGS heat exchangers experience high stresses, indicating that a design approach considering also the stress evaluation is of great importance.

The objective of this paper is to present a method to design a header and coil SGS accounting for its dynamic performance, stress sensitivity and impact on the power plant techno-economic performance. A parabolic trough power plant with thermal energy storage was considered. The work builds on the previous work of the authors [18] and aims at expanding it by including these additional analyses. The method presented in this paper allows for selecting the optimal SGS design for a given power plant design and operating conditions. The SGS dynamic models were validated against operational data of an existing power plant. The thermodynamic and economic calculations were coupled with a multi-objective optimization framework in order to minimize both water pressure drop and purchase equipment costs (PEC). In order to show the relevance for practical applications, the proposed design method was applied to an existing PTPP configuration. In the first step, the performance of the optimal designs belonging to the Pareto front of the optimiza-

tion procedure was analysed by calculating the levelized cost of electricity (LCOE) of the PTPP. Secondly, each design was tested for the thermo-mechanical stress calculation. The optimal SGS design was chosen by analyzing both the LCOE and stress indicators.

This is the first paper presenting an integrated method which incorporates the low-cycle fatigue requirements, transient stress evaluation and power plant performance in the design procedure of steam generator systems. As compared to the works previously mentioned [17, 39], the novel contribution of this work is to include the thermo-mechanical stress indicator into the design procedure of the SGS. This is done by excluding the optimal designs belonging to the Pareto front, which present high stresses or do not comply with the norms. Both Pelagotti et al. [17] and Gonzalez-Gomez [39] analysed the stress evolution for a given SGS design, but did not evaluate how different optimal designs would perform from a thermo-mechanical standpoint. The results of this paper can impact both the industry and the scientific community. From and industrial standpoint, the results point out optimal solutions for a particular CSP configuration, but the overall method can also be applied for improving the current solutions. At a research level, the paper can be considered as a milestone towards the design guidelines for components installed in highly transient power plants, such as CSP plants.

In Section 2, the paper presents the methods used to evaluate the power plant performance and the design procedure of the SGS and its dynamic performance evaluation in terms of start-up and thermo-mechanical stresses. Furthermore, it presents the multi-objective optimization method and the constraints applied to obtain feasible solutions. Section 3 presents and discusses the results of the validation and multi-objective optimization and the impact of the different optimal designs on the LCOE and total stresses during start-up procedures. Section 4 outlines the conclusions and final remarks.

2. Methods

This section explains the methods employed for carrying out the modelling tasks. As the results from the system and component level analysis are interdependent, the optimization process takes into consideration constraints and boundary conditions of both levels.

2.1. Power plant modelling

The modelled power plant is based on a PTPP with an air cooled condenser as presented by the authors in a previous work [8]. The main difference compared with the layout presented in Ref. [8] is the two-fold split arrangement of the re-heater which is composed by two

heat exchangers parallel to the superheater and economizer, respectively. This configuration allows for lower temperature gradients in the re-heater tubes, thus resulting in lower thermal stresses [19]. Figure 1 shows a scheme of the considered power plant and the placement of the heat exchangers.

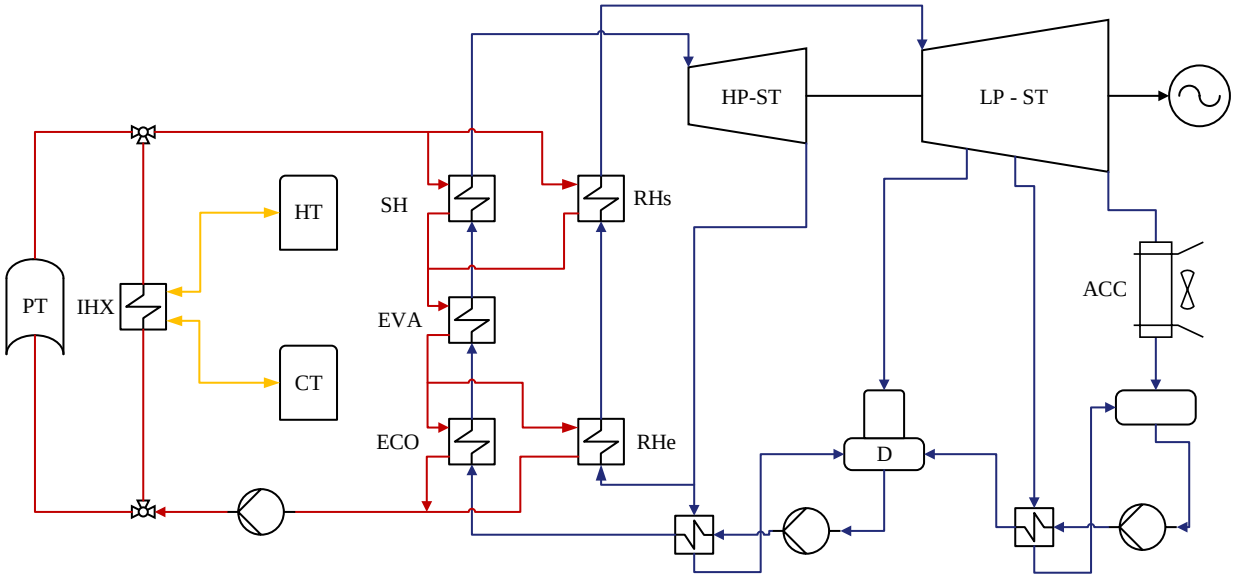

Figure 1: Parabolic trough power plant layout.

The red lines indicate the HTF (Terminol-VP1) loop, whose temperature is raised by the parabolic trough (PT) collectors. The fluid is then pumped directly to the steam generator system. This comprises the economizer (ECO), evaporator (EVA), superheater (SH) and two re-heaters (RH). The blue line cycle indicates a regenerative Rankine-reheat cycle with high pressure (HP) and low pressure (LP) steam turbines (ST), an air cooled condenser (ACC) and a deaerator (D). The yellow lines represent the flow of the molten salt coming from and to both the hot tank (HT) and cold tank (CT) and which can exchange heat with the HTF through the indirect heat exchanger (IHX).

The power plant modelling was performed in DYESOPT (DYnamic Energy System OPTimizer), a tool developed and validated at KTH, Royal Institute of Technology, Stockholm [40]. The tool performs the design of the power plant at nominal state, evaluates the transient performance and estimates techno-economic indicators. Figure 2 shows the logic flow of information and calculations within the tool, where the grey and black boxes represent the inputs and outputs of the model, respectively. The PTPP model was developed by the authors and previously validated, with a maximum deviation of -3.7 % for the yearly electricity production [41].

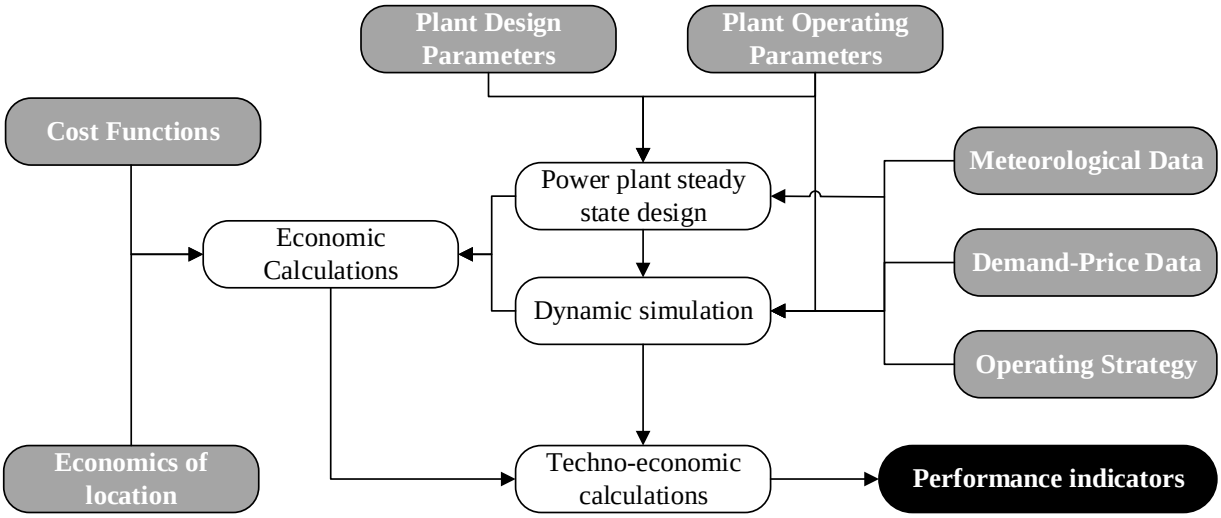

Figure 2: DYESOPT logic flow of information. Grey and black boxes represent the inputs and outputs of the model, respectively.

The nominal load design of the components was carried out in Matlab [42]. The results of the design were coupled with the yearly transient performance evaluation, which was performed using TRNSYS [43]. The models are zero-dimensional to reduce computational requirements [44]. The off-design performance of the heat exchangers was modelled using exponential scaling functions of the UA values (overall heat transfer coefficient times area), with respect to the mass flow ratio at off-design and design. The Stodola [45] equation was used to model the turbine off-design behavior. The parabolic trough solar field model takes into account both the optical losses related to the sun position and geometry of the collectors and the thermal losses due to the expansion vessel and piping [46–48]. The results were post-processed in Matlab to get the chosen performance indicators. Cost functions and economics specific to the location and power plant were taken into account if economic indicators were to be calculated.

The levelized cost of electricity (LCOE) was chosen as the power plant economic indicator, as expressed in Equation 1. The CRF is the capital recovery factor, which, as expressed in Equation 2, depends on the real interest rate (i), the considered plant lifetime and the annual insurance rate (k_i). The CAPEX refers to the capital expenditure, which takes into account direct (purchase and installation) and indirect (land, taxes and engineering) costs related to each component. The OPEX refers to the operational expenditures, which comprise operation and maintenance costs such as labor, service, utility, consumables and other miscellaneous. In this paper, the plant lifetime was assumed to be 25 years, with

a real debt interest rate of 6 % and an annual insurance rate of 0.25 % according to Ref. [40]. CAPEX and OPEX were calculated following the method presented in Ref. [40], while the SGS investment cost was estimated more in detail by following the method previously presented by the authors in Ref [18]. The main inputs required for designing the PTPP are summarized in Table 1. Different storage sizes were analysed to investigate the impact of the SGS dynamic performance on the LCOE calculations, as higher storage size would mean lower load changes and fewer start-up procedures throughout the year.

$$LCOE = \frac{CRF \cdot CAPEX + OPEX}{E_{\text{gen,yr}}} \tag{1}$$

$$CRF = k_{\text{i}} + \frac{i \cdot (1+i)^{N_{\text{years}}}}{(1+i)^{N_{\text{years}}} - 1} \tag{2}$$

Table 1: Parabolic trough power plant design parameters

SGS design parameters	Units	Values
Solar multiple (SM)	[-]	2
Gross power	[MW]	55
TES capacity	[h]	5/7.5/10
Inlet HP/LP pressure	[bar]	100/16.7
Nominal condensing pressure	[bar]	0.06
SF HTF maximum temperature	[°C]	393
SF HTF outlet temperature	[°C]	293
Nominal turbine inlet temperature	[°C]	378

2.2. Steam generator system modelling approach

The SGS is made of two parallel lines of heat exchangers which include a SH, ECO, EVA and two RHs [16]. Figure 3 depicts the geometry of the evaporator, while Figure 4 illustrates the geometry of single-phase heat exchangers, which was simplified as parallel tube banks. A detailed heat exchanger arrangement is depicted in Figure 7. In the single-phase heat exchangers, the heat transfer fluid flows on the shell-side. In the evaporator, the HTF flows on the tube-side and the heat transfer is characterized by pool boiling on the shell-side. The water flows in the tubes for all the other heat exchangers. The red and blue lines represent the heat transfer fluid and water flows, respectively. The HTF flows through the SGS to supply the thermal energy to increase the temperature of the inlet subcooled water to the required temperature at the turbine inlet. The low pressure steam, coming

from the extraction, is heated up in the two re-heaters to the desired re-heat temperature at the turbine inlet.

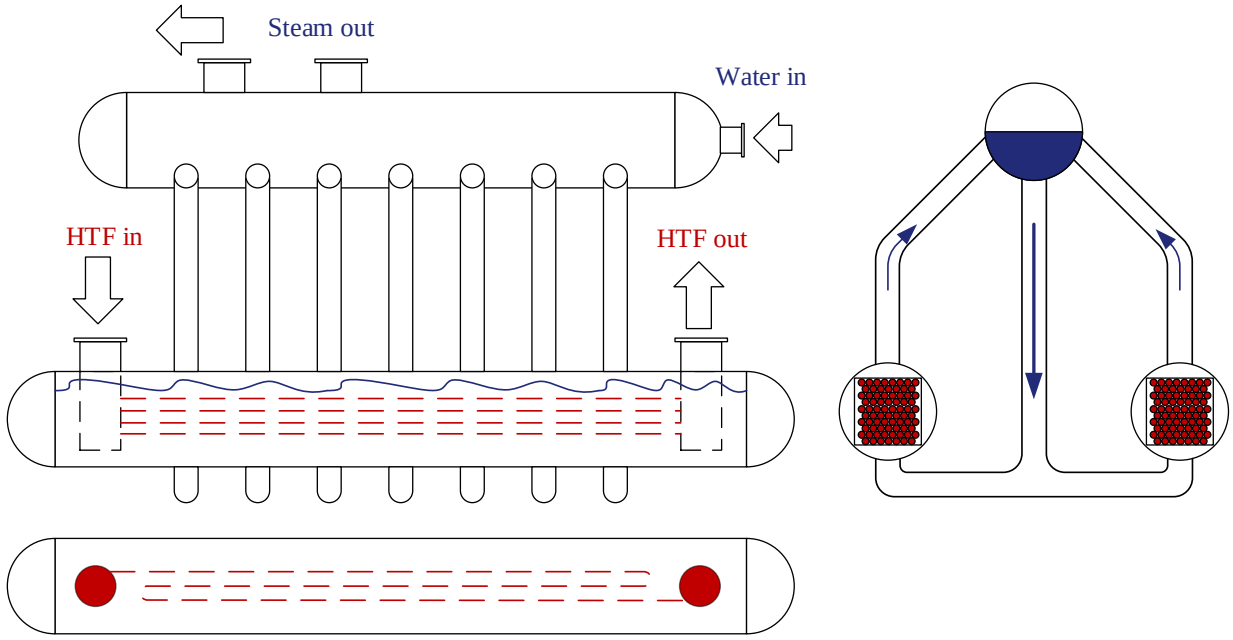

Figure 3: Header and coil shell recirculation evaporator. Front view (top), top view of the heat exchanger (bottom), side view (right).

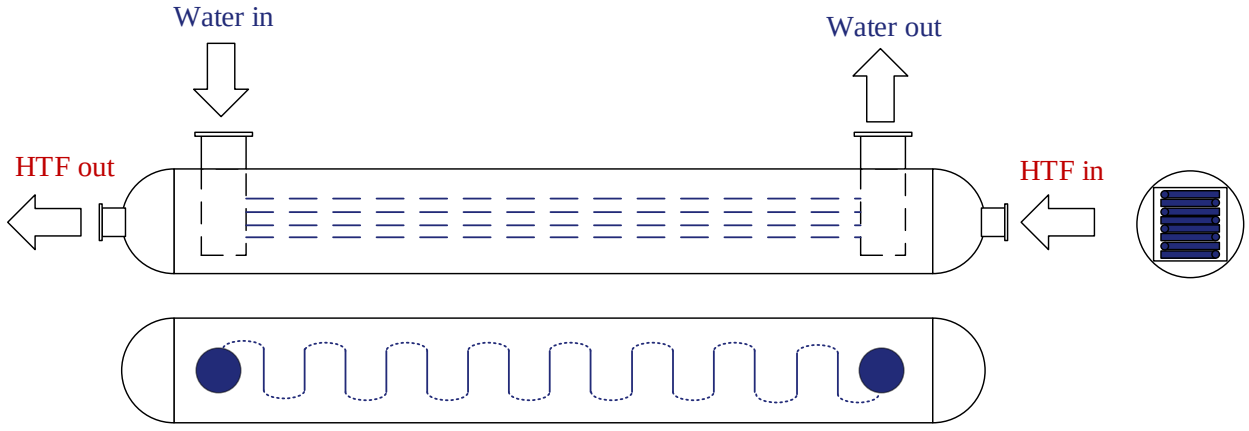

Figure 4: Header and coil shell single-phase heat exchangers geometry. Front view (top), top (bottom), side view (right).

The evaporator consists of two separate heat exchangers in order to reduce the size of the headers and shells. Natural circulation allows for the flow between the steam drum and the heat exchangers. Figure 5 illustrates the necessary steps to design the steam generator and perform the transient performance analysis. In order to carry out the SGS design,

power block data and operating constraints are the required inputs together with price data, if economic calculations are considered. The results of the design yield the basis for the low-cycle fatigue calculations according to the EN12952-3 [12]. This determines the maximum allowable heating rates in order to guarantee a set lifetime. If the constraints are not satisfied, the geometry inputs are modified until the requirements are met.

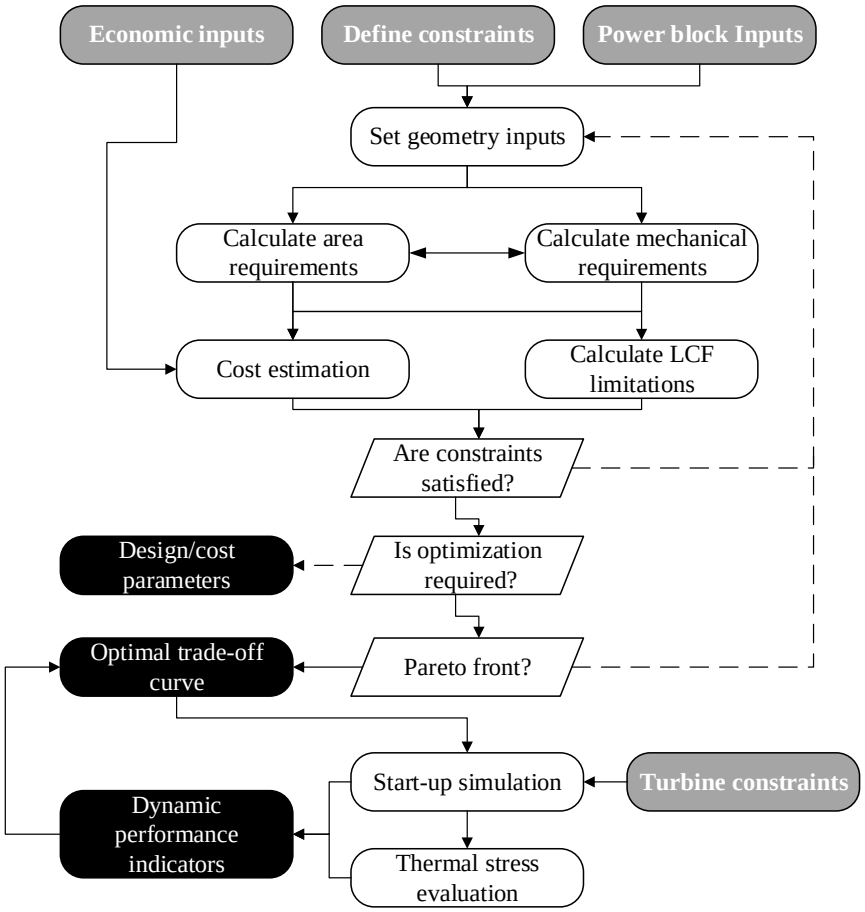

Figure 5: Steam generator system design and dynamic simulation method workflow. Solid lines represent a YES logic, while dashed lines represent a NO logic. Grey and black boxes represent the inputs and outputs of the model, respectively.

The model is linked to a multi-objective optimizer already implemented in the Matlab toolbox [42]. At the beginning of the optimization, conflicting objectives, which are either minimized or maximized, are set. Both design specifications and operation parameters can be defined to allow for variations within the limits chosen for the study. The algorithm carries out as many iterations as required to conclude the optimization and achieve an optimal trade-off curve or Pareto front [49]. Further details about this part of the method may be found in a previous work by the authors [18]. Once the design routine is finished,

the geometrical results are used in the dynamic simulation model. The start-up procedure is simulated in Dymola [50], and the results serve as a basis for the stress calculations. The transient start-up results are interpolated to determine the proper scaling power coefficients of the UA scaling functions, necessary for the TRNSYS model.

The optimization of the design at nominal load follows the same approach as that presented by the authors in a previous work [18], with the objective to minimize at the same time both the associated purchase equipment cost (PEC) and the total water pressure drop. The boundary SGS design parameters derived from the design of the power plant are presented in Table 2. The optimization constraints and variables are indicated in Tables 3 and 4 according to Ref. [8]. The tube outer diameter was defined as a discrete variable, with the possibility to select commonly available diameters in industry, according to Coulson et al. [51]. The four choices, referenced as indexes in Table 4, were 25 mm, 30 mm, 38 mm and 50 mm. The velocities were constrained in order to avoid fouling and excessive erosion [51], while the maximum steam velocity was calculated according to the charts by Merrit et al. [52], which are dependent on the operating pressure. All the heat exchanger components are assumed to be made of carbon steel [53].

Table 2: Steam generator system design parameters

Parameters	**Units**	**Value**
Turbine inlet temperature	[°C]	377.6
Turbine inlet pressure	[bar]	100
Reheat outlet temperature	[°C]	378.9
Inlet pressure at reheat	[bar]	16.7
Inlet temperature at reheat	[°C]	204.4
Feedwater temperature	[°C]	245.94
HTF inlet temperature	[°C]	393.3
HTF inlet pressure	[bar]	15
Steam mass flow rate	[kg/s]	60.988

Table 3: Optimization constraints

Parameter	Unit	Value
Tube minimum velocity	[m/s]	0.5
Tube maximum velocity	[m/s]	4
Shell minimum velocity	[m/s]	0.2
Shell maximum velocity	[m/s]	1.5
Steam maximum velocity	[m/s]	25
Oil maximum pressure drop	[bar]	2
Evaporator minimum heating rate	[K/min]	8.5
Super-heater minimum heating rate	[K/min]	15
Minimum drum internal diameter	[mm]	1500

Table 4: Optimization decision variables

Variables	Unit	Lower boundary	Upper boundary
Tube outer diameter index	[-]	1	4
Number of layers	[-]	20	40
Number of tubes per layer	[-]	3	15
Riser outer diameter	[mm]	200	300
Number of risers	[-]	5	15

2.3. Steam generator transient modelling

The transient modelling was carried out using Modelica [50], which is an effective object-oriented language to develop models by using a modular approach. Existing and validated libraries of reusable models can be employed to carry out the specific modelling tasks as they can be modified and tailored to the needs of the particular case. In this work, the ThermoPower [54] library was chosen to carry out the transient modelling of the heat transfer for both the single-phase heat exchangers and the natural circulation evaporator.

All of the heat transfer blocks are based on mass, energy and momentum balances as shown in Equations 3, 4 and 5, where ρ is the density of the fluid, A is the cross-sectional area, x is the spatial coordinate, t is the time and v is the velocity. Equation 4 depends also on the specific enthalpy h, wetted perimeter ω and the entering heat flux φ. As for Equation 5, the additional parameters p, C_{f}, g and z are the pressure, fanning factor, constant of gravity and vertical coordinate, respectively. More detailed information can be found in Ref. [55] and Ref. [54]. The two phase flow region is solved using the mean density method [56]. The equations are solved with the finite volume method (FVM) and a staggered alignment [57]. The modified Dassl solver [58] is used to resolve the algebraic system of equations.

$$\frac{d}{dt}(\rho A) + \frac{\partial}{\partial x}(\rho A v) = 0 \tag{3}$$

$$(\rho A)\frac{\partial h}{\partial t} + (\rho A v)\frac{\partial h}{\partial x} - A\frac{\partial p}{\partial t} = \omega\varphi \tag{4}$$

$$\frac{d}{dt}(\rho v A) + A\frac{\partial \rho v^2}{\partial x} + \rho g A\frac{dz}{dx} + \frac{\omega C_{\mathrm{f}}}{2}(\rho v \mid v \mid) = 0 \tag{5}$$

A high number of tube coils (>6) allows for simplifying the modelled geometry and applying a counter-current flow configuration [30]. The heat transfer coefficients and pressure drop calculations followed the method proposed in Ref. [18]. The only modification was applied to the heat transfer coefficient on the pool boiling side. It was calculated using the Jens and Lotte correlation [59] in order to save computational time, as it requires a lower number of thermodynamic property calculations as compared to the more detailed correlations such as the one suggested by Stephan-Abdelsalam [59]. This simplification is justifiable as the overall heat transfer performance is governed primarily by the heat transfer coefficient on the HTF side [60]. The evaporator flow configuration, on the other hand, was modelled following a similar approach to that presented by Benato et al. [61], see Figure 6. Each water control volume (Nw) is associated with the corresponding tube control

volume (Nt) representing a 2D geometry. The total number of control volumes depends on the number of coils (Nc) as well as on the number of discretization volumes in the tube perpendicular direction (Nv).

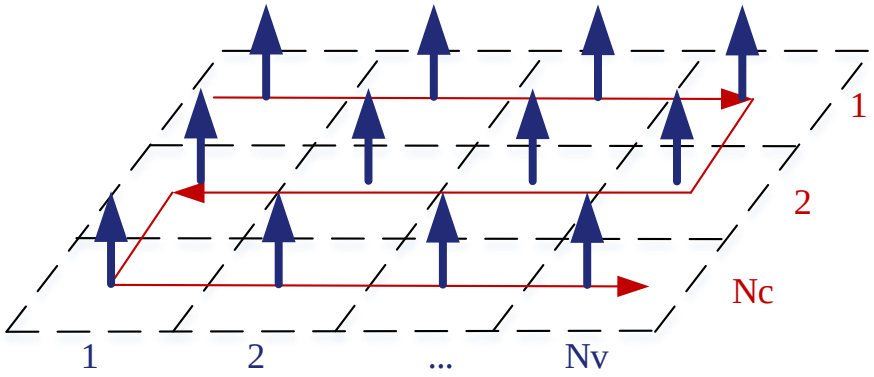

Figure 6: Two phase flow geometrical approach for the finite volume method.

The steam drum is modelled according to the method presented by Åstrom and Bell [62] (as already implemented in ThermoPower) with the energy and mass conservation equations as shown in Equations 6 and 7. The steam drum heat loss coefficient was calculated following the method presented by Churchill et al. [63] for natural convection on horizontal cylinders. The natural circulation loop between the heat exchanger and steam drum is closed by the risers and downcomer, whose models take into account pressure drops. For a given tube number, height and diameter, the riser/downcomer mass flow rate is determined in order to balance the driving pressure force resulting from the density gradient between the two-phase mixture in the riser and liquid phase in the downcomer and the frictional pressure drop due to the length and singularities in the tubes [64].

$$\frac{d}{dt}\left(\rho_{\mathrm{v}} V_{\mathrm{v}} + \rho_{\mathrm{l}} V_{\mathrm{l}}\right) = \dot{m}_{\mathrm{l}} - \dot{m}_{\mathrm{v}} \tag{6}$$

$$\frac{d}{dt}\left(\rho_{\mathrm{v}} V_{\mathrm{v}} h_{\mathrm{v}} + \rho_{\mathrm{l}} V_{\mathrm{l}} h_{\mathrm{l}} - p V_{\mathrm{t}} + m_{\mathrm{t}} C_{\mathrm{p}} T_{\mathrm{m}}\right) = \dot{m}_{\mathrm{l}} h_{\mathrm{l}} - \dot{m}_{\mathrm{v}} h_{\mathrm{v}} + \dot{Q} \tag{7}$$

2.4. Start-up constraints and control strategy

Figure 7 presents the SGS layout, with details including bypass valves and controller configurations. The blue and red solid lines represent the water and HTF flows, respectively.

The green and orange dashed lines follow the control signal of the two controllers (C1 and C2), while the black dashed lines represent the process variable (PV) signals which are measured at the steam drum, superheater and re-heater.

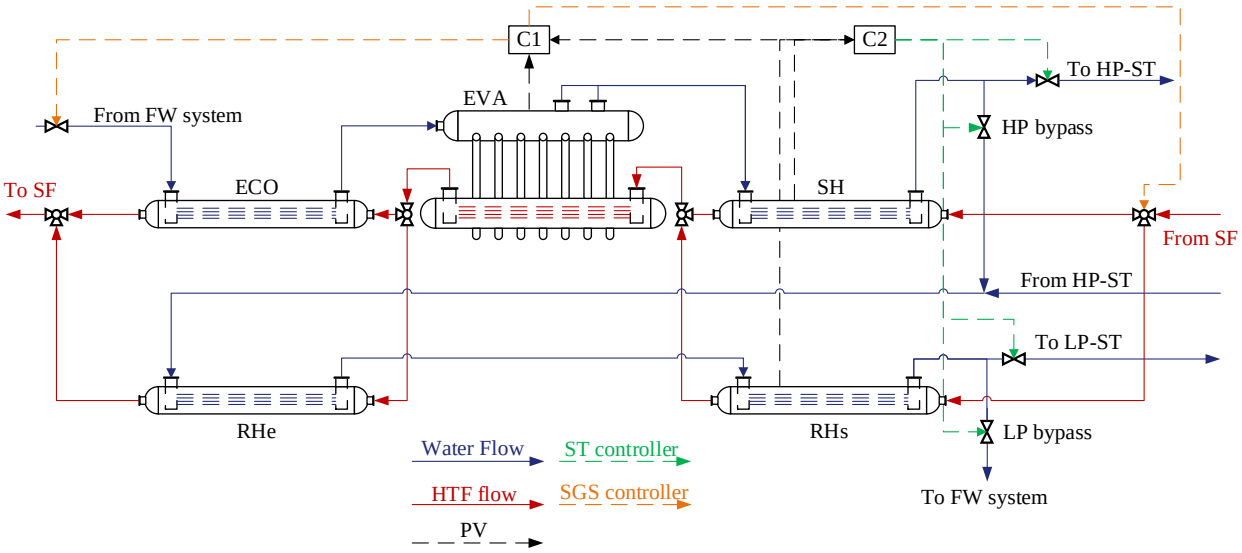

Figure 7: Heat exchanger configuration of the steam generator system and details of control logic information and bypass valves.

The steam generator start-up control logic is presented in Figure 8, which is managed by the C2 controller illustrated in Figure 7. The presented control strategy is based on Refs. [65, 66] and adapted to the specific case considered. The procedure is initiated when the HTF temperature reaches a sufficiently high value (280 °C) (as indicated by (1) in Figure 8). The C2 controller monitors the steam pressure, hence the allowable v_T for both the evaporator and superheater, and sets the HTF temperature and mass flow rate. The C1 controller monitors the water level in the steam drum and sets the feedwater flow to the economizer. The HTF is then pumped to the SGS with a mass flow rate kept at 10 % of its nominal value in order to minimize heat losses [66]. By acting on the high pressure steam turbine (HP-ST) opening valve, the pressure is kept at the minimum acceptable value of the steam turbine (26 bar). While the HTF and steam temperatures increase, the steam mass flow rate is bypassed and redirected to the condenser until acceptable values for the turbine are reached (a minimum degree of superheat needs to be achieved, as for the start-up curves provided by the manufacturer).

At a certain point the minimum acceptable steam temperature is reached, whereby the inlet HP-ST valve is opened. At a mass flow rate to the steam turbine of 3 % to 5 % of

its nominal value, the roll-up phase and synchronization (see (2) in Figure 8) are initiated. During this phase, whose duration depends on the turbine start-up mode (cold, warm or hot), any steam mass flow rate exceeding the minimum values is bypassed and sent to the feedwater system. Once the roll-up is finished, the HP-ST valve is opened, and both the mass flow rate and the pressure are increased. The HTF flow rate is then increased by following the heating rate constraints of the steam drum; see (3) in Figure 8. Once the mass flow rate, temperature and pressure reach their nominal values, the SGS start-up phase is finished. In order to avoid swelling and dry-out, the feedwater mass flow rate was controlled by an additional controller (C1) which manages the water level in the drum around the center line. Both controllers were integrated in proportional integral derivative (PID) controllers which were calibrated following the Ziegler-Nichols method [67].

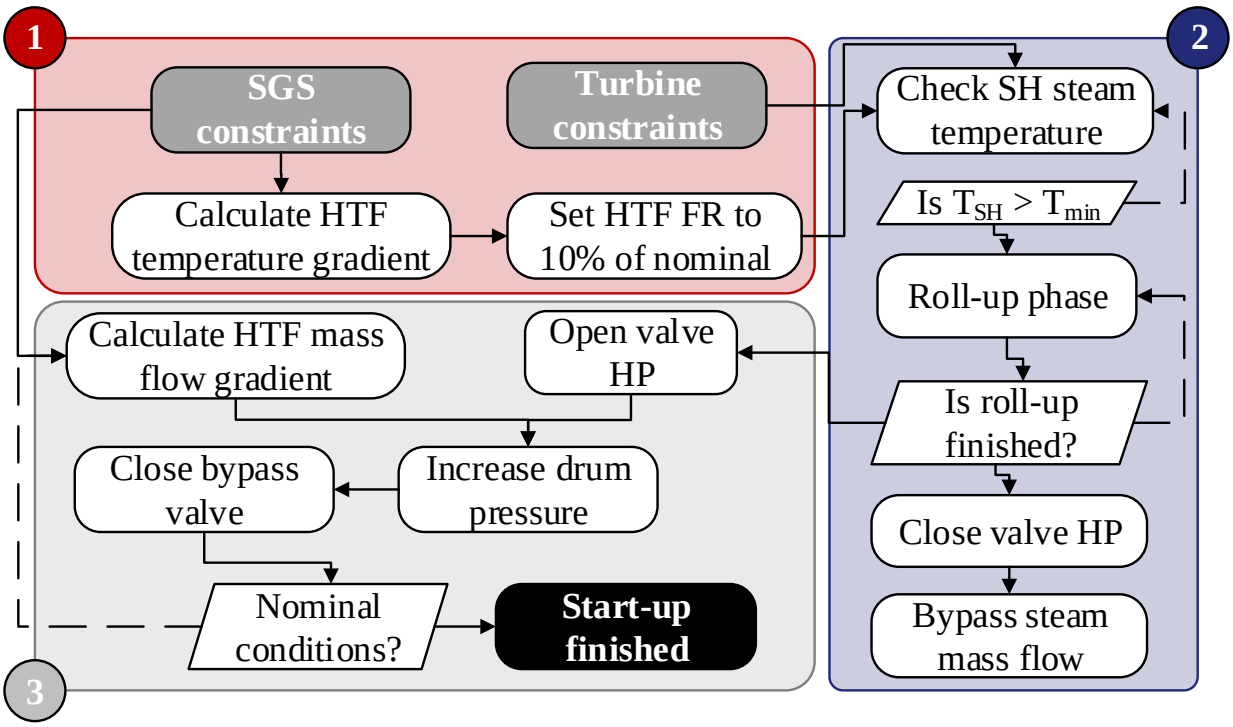

Figure 8: Steam generator system start-up logic. Solid lines represent a YES logic, while dashed lines represent a NO logic. Grey and black boxes indicate inputs and outputs, respectively.

2.5. Stress evaluation in materials

The total stress in the heat exchanger materials results from the addition of both thermal and pressure stresses as illustrated in Equation 8 [12]. The stress resulting from the pressure component depends on a concentration factor α_M which is computed according to

the EN 12952-3 and depends on the ratio of the diameter to the thickness of the components forming the junction. D and t represent the average diameter and thickness of the geometry considered. The thermal stresses depend on the thermal concentration factor α_{T} which is calculated according to the working fluid phase (vapour or liquid) and the diameter ratio of the main components, the Young's modulus E, the thermal expansion coefficient β and the Poisson ratio ν. T_{i} represents the internal fluid temperature, while T_{m} represents the mean integral metal temperature.

The header wall temperature profile was calculated according to Equation 9, representing the cylindrical heat diffusion equation in the radial direction only, with initial condition and third kind boundary conditions in terms of the convective heat transfer coefficient. The equation was discretized radially and solved using the Skeel method [68], which was already implemented in the Matlab toolbox. The outer heat transfer coefficient was calculated using the Churchill correlation [69] for external forced convection on cylinders, while the internal h was calculated using the Gnielinski correlation [69]. This definition of boundary equations was set to account for the non-negligible heat transfer resistance experienced by the fluid, especially at part-load conditions, as the heat transfer coefficient can become very low (below 200 W/m^{2}K) for low mass flow rates). In the case of the steam drum, the internal boundary condition was different and set as a Dirichlet boundary condition, setting the internal metal temperature equal to the water temperature as suggested by Kim et al. [70]. The outer heat transfer coefficient was calculated using the Churchill correlation [63] for natural convection on horizontal cylinders.

$$\sigma = \sigma^P + \sigma^T = \alpha_{\mathrm{M}} \frac{D}{2t} \cdot p + \alpha_{\mathrm{T}} \frac{E\beta}{1-\nu} (T_{\mathrm{m}} - T_{\mathrm{i}}) \tag{8}$$

$$\begin{cases} \dfrac{1}{\alpha}\dfrac{\partial T}{\partial r} = \dfrac{1}{r}\dfrac{\partial}{\partial r}\left(r\dfrac{\partial T}{\partial r}\right) \\ T(r,0) = T_0 \\ -\lambda \left.\dfrac{\partial T}{\partial r}\right|_{r=r_i} = h_i(T_i - T(r_i,t)) \\ -\lambda \left.\dfrac{\partial T}{\partial t}\right|_{r=r_o} = h_o(T(r_o,t) - T_o) \end{cases} \tag{9}$$

With regards to the EN 12952-3, the maximum and minimum allowable stresses are set in order to protect the magnetite layer on the metal wall of the components. The former was

set to be calculated 200 MPa above the pressure stress at the nominal operating condition, while the latter was set to be 600 MPa below the pressure stress at the nominal operating condition.

2.6. Model validation

The nominal load design model was validated previously by the authors in Ref. [18], with a maximum relative deviation (in absolute value) for the estimated total weight of -3.6 %. The SGS PEC estimation was also validated with a confidence range of ±2 %. In order to evaluate the reliability and accuracy of the developed dynamic model, a validation was performed both for nominal steady state and transient conditions.The data used for the validation was obtained by measurements of the working conditions of an operating parabolic trough power plant, located in India.

The steady state validation was performed by comparing the main thermodynamic parameters (steam mass flow rate, pressure and temperature, HTF outlet temperature) at nominal load with the data available of an existing power plant. The predictive performance of the dynamic model was evaluated by comparing its results with transient operational data of the power plant. The following six parameters were the available measured data for the validation: superheater steam outlet temperature and pressure, steam mass flow rate, feedwater mass flow rate, re-heater steam outlet temperature and HTF outlet temperature. These parameters also represent the main output of the SGS model. The HTF inlet mass flow rate and temperature, economizer water inlet temperature and re-heater water inlet mass flow-rate, pressure and temperature are the inputs to the model. In order to quantify the predictive performance of the models, the following parameters were calculated:

$$IRE = \frac{\int_0^{\text{time}} (y_{\text{model}} - y_{\text{data}})\ \mathrm{d}t}{\int_0^{\text{time}} (y_{\text{data}})\ \mathrm{d}t} \tag{10}$$

$$RMSE = \sqrt{\left(\frac{\sum_{\text{i=1}}^{\text{N}} (y_{\text{model}} - y_{\text{data}})^2}{N} \right)} \tag{11}$$

$$NRMSE = \frac{RMSE}{y_{\max} - y_{\min}} \tag{12}$$

The integral relative error (IRE) represents an overall accuracy measure over the simulation time considered. For example, if the calculations are applied to the mass flow rate, the IRE will give an estimation of the deviation of the mass produced over the interval considered. The root mean squared error ($RMSE$) and normalized RMSE ($NRMSE$) provide a measure of the instantaneous accuracy of the model, in absolute and relative terms, respectively. The y maximum (max) and minimum (min) values refer to the model results and data points for a number of available points (N).

3. Results and discussion

3.1. Model validation

This section presents the validation both for steady state operation at design point/nominal load and for dynamic operation. Table 5 presents the results of the validation of the main parameters at steady state nominal load.

Table 5: Steady-state nominal validation.

Parameter	Units	Model	Data	Relative deviation
SH degree of superheat	[° C]	73.40	71.40	2.80%
RH degree of superheat	[° C]	207.01	206.61	0.19%
SGS HTF outlet temperature difference	[° C]	92.33	92.30	0.03%
FW mass flow rate	[kg/s]	36.60	36.89	-0.79%
EVA steam outlet mass flow rate	[kg/s]	36.60	36.89	-0.79%
SH steam outlet pressure	[bar]	103.96	104.00	-0.04%

The maximum deviation is found for the superheater degree of superheat (2.8 %) which is attributed to the underestimation of the steam mass flow rate by 0.79 %, as a lower mass flow rate would determine a higher superheated steam temperature for the same heat input. All the other parameters present a deviation below 1 %. The operational data of the power plant for a day in March 2014 between 8:15 and 18:15 are depicted in Figure 9. These data are used as input for the dynamic simulation model. Figure 9a presents the total HTF mass flow rates and the split between the superheater and re-heater mass flow rates, Figure 9b illustrates the HTF inlet temperature and Figure 9c presents the water inputs required by the model, such as the economizer inlet temperature and the re-heater inlet temperature and pressure.

The results of the dynamic validation are presented in Figure 10. Figures 10a, 10b, 10c, 10d, 10e and 10f present the temperatures of the steam at the superheater outlet, re-heater

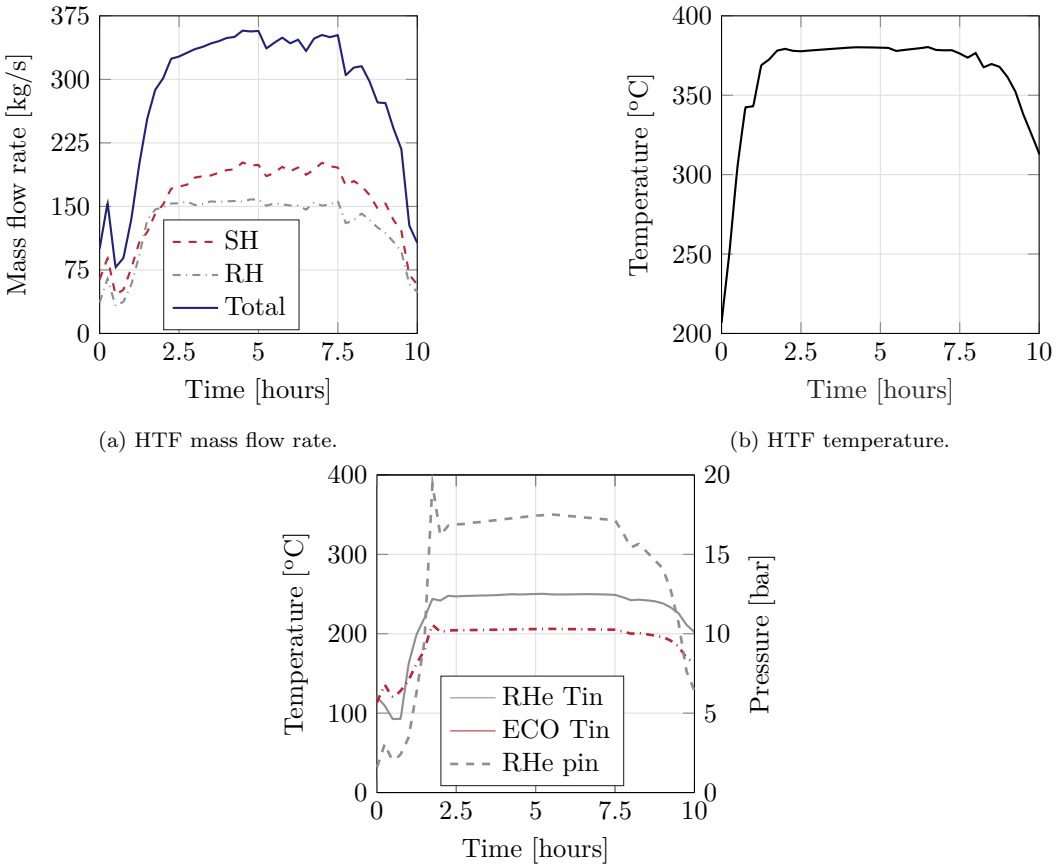

(a) HTF mass flow rate.

(b) HTF temperature.

(c) Economizer water inlet temperature and re-heater steam inlet temperature and pressure.

Figure 9: Power plant operational data. Inputs for the validation of the dynamic model.

outlet and HTF outlet, the feedwater and steam mass flow rate and pressure, respectively. The results suggest that the superheater and HTF outlet temperatures are well represented by the model, with the latter being overestimated by 1.4 % on average between 2.5 h and 7.5 h from the start of the simulation. This can be explained by the fact that the steam mass flow rate is underestimated; see Figure 10e. The re-heater steam outlet temperature is properly represented after 2.5 hours, whereas it is overestimated before this time. This is mainly linked to the fact that the temperature sensor is placed after the spray attemperator before the low pressure steam turbine (LP-ST) inlet, while the model provides the results for the SGS outlet. The difference between the model and the data results can be linked to the thermo-mechanical constraints of the steam turbine during the start-up, as lower steam temperatures are acceptable during this procedure. Concerning the water mass flow rates, the feedwater model results predict less fluctuations than presented in the plant data.

This can be attributed to the noise occurring in the process variable signal and difficulties in measuring the water density and the drum level [71]. Both aspects are not taken into account in the model. If between the 1 h and 5 h simulation times, the feedwater mass flow rate is overestimated, the steam mass flow rate and pressure are underestimated. This is due to the fact that a higher mass flow rate of subcooled water, hence with low enthalpy value, enters the steam drum, therefore decreasing the energy value of the water in the steam drum. This is in turn translated into lower pressure and mass flow rate values for the outlet steam.

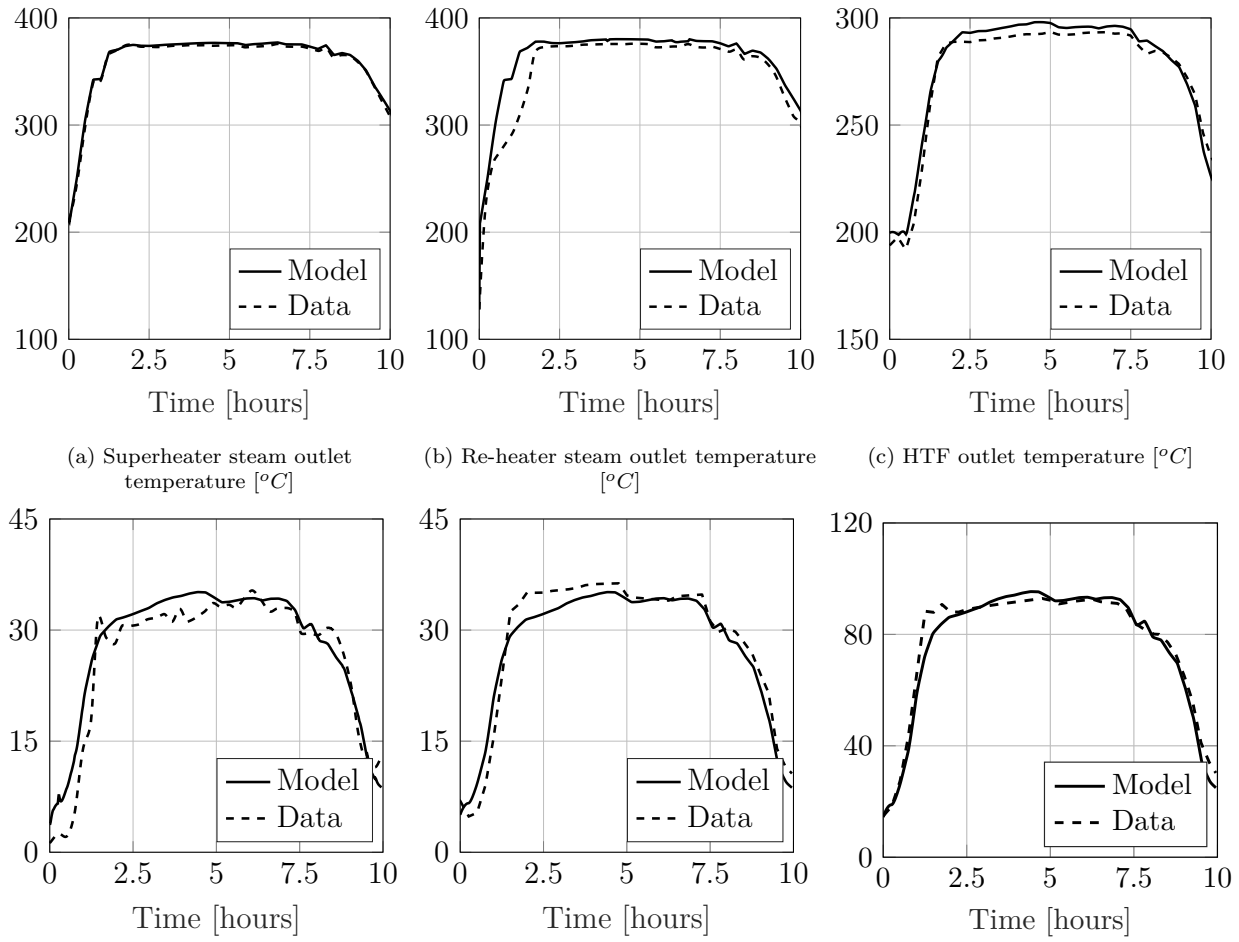

(a) Superheater steam outlet temperature [^oC]

(b) Re-heater steam outlet temperature [^oC]

(c) HTF outlet temperature [^oC]

(d) Feedwater mass flow rate [kg/s]

(e) Steam mass flow rate [kg/s]

(f) Superheater outlet steam pressure [bar]

Figure 10: Model validation results for transient operation. Comparison with power plant operational data.

All of these considerations are summarized and quantified in Table 6 where the three indicators described in Section 2.6 are presented. The highest IRE and NRMSE are found for the RHs steam outlet temperature and FW mass flow rate. All the six parameters

considered present a relative integral and instantaneous deviation below 9 %, indicating that the dynamic model captures the main characteristics of the thermodynamic parameters of the plant during dynamic operation adequately and with sufficient accuracy for the purposes of the present paper.

Table 6: Transient validation results.

Parameter	Units	IRE [%]	RMSE [Unit as the quantity considered]	NRMSE [%]
SH steam outlet temperature	[° C]	0.54	2.37	1.43
RH steam outlet temperature	[° C]	3.36	18.98	7.65
SGS HTF outlet temperature	[° C]	0.83	3.85	3.80
FW water mass flow rate	[kg/s]	5.29	2.78	8.14
EVA steam outlet mass flow rate	[kg/s]	-2.80	2.06	6.54
SH steam outlet pressure	[bar]	-1.33	3.77	4.84

3.2. Design optimization

The optimization was carried out as previously presented in Section 2.2, with the objective of minimizing the associated PEC and total water side pressure drop, while imposing constraints as presented in Section 3.2. Once the multi-objective optimization results were obtained, all the design points of the Pareto front were used to evaluate the LCOE of the PTPP, ensuring that the total stress values at the sensible junctions are within the allowable limits. Figure 11 depicts the multi-objective optimization results for the SGS design.

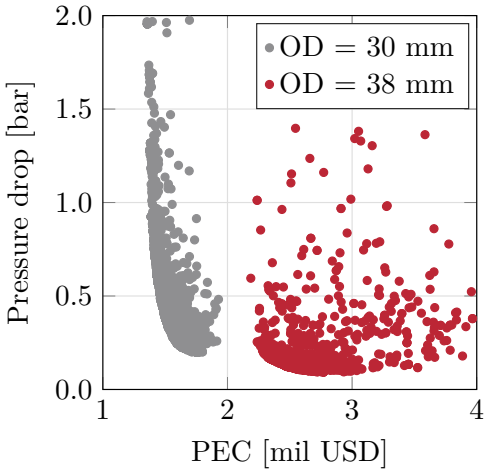

Figure 11: Multi-objective optimization results for the design of the steam generator system.

The figure indicates that outer diameters (OD) of 30 mm and 38 mm represent the optimal solutions for high and low water pressure drops, respectively. The 25 mm and 50 mm solutions resulted in non-optimal designs, since these diameters are associated with high pressure drops and low maximum allowable heating rates, respectively. In order to select the most suitable design on the Pareto front, the optimal designs were evaluated with respect to the power plant LCOE, and maximum stresses ($\sigma_{\max}$) and stress variations ($\Delta\sigma = \sigma_{\max} - \sigma_{\min}$) during the start-up phase. High $\Delta\sigma$ causes shorter expected lifetime according to the LCF calculations [72]; therefore, it is preferable to choose the geometrical configurations which would lead to lower stress variations. These two indicators, which were normalized against the ultimate tensile strength (UTS), are presented in Figures 12a and 12b for both the inlet and the outlet header of the superheater. The results of the stresses in the drum are not presented in the figure as they are the same for all the SGS designs. This is because the results of the optimization indicate that a single drum/downcomer configuration is optimal, therefore not affecting the stress results for the different optimal designs. The impact of the different designs on the power plant LCOE is shown in Figure 12c. These are presented in terms of relative increase as compared to the design which results in the lowest LCOE. The TES values are chosen according to an existing PTPP installation [73] and relative change in the range of ± 33 %, in order to analyze the influence of the storage size.

The results shown in Figure 12 indicate that the optimal solutions with water pressure drops lower than 0.8 bar present higher LCOE, higher maximum stress differences and higher maximum stresses below 0.4 bar. Figure 11 indicates that the 38 mm outer diameter solution allows for a pressure drop below 0.4 bar and, therefore, these considerations allow for excluding the 38 mm outer diameter solution, as the associated decrease in parasitic consumptions, due to lower SGS pressure drops, does not compensate for the associated higher PEC and slower dynamic response (the further to the right, the higher the SGS total metal mass and volume). The results shown in Figure 12 indicate that the design which presents the highest total water pressure drop presents the lowest LCOE. Furthermore, such design presents the lowest maximum stress for both headers and low maximum stress difference. These findings justify the selection of the highest pressure drop solution as the optimal design for the considered power plant. Lower LCOEs are obtained for higher pressure drops. The reason is that lower parasitic consumption associated with lower pressure drops does not compensate for the higher associated PEC and slower dynamic response of the SGS (the lower the pressure drop, the higher the SGS total metal mass and volume due to

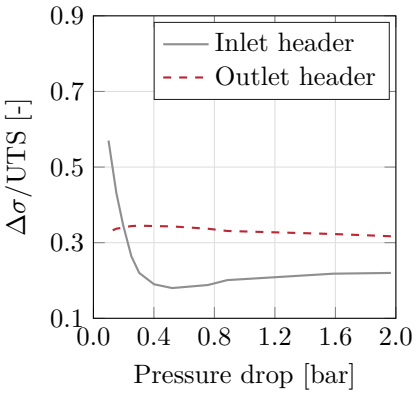

(a) Headers' maximum stress difference.

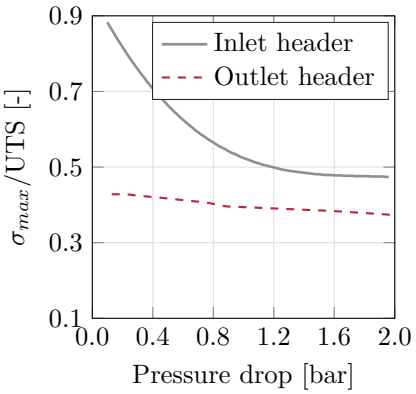

(b) Headers' maximum stress.

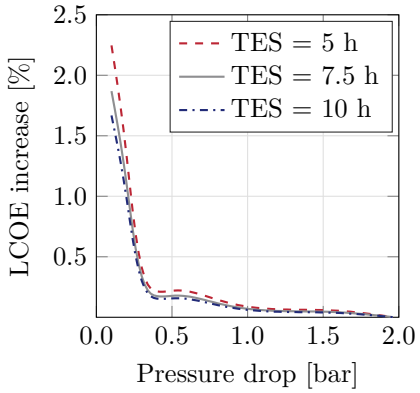

(c) Power plant LCOE increase.

Figure 12: Optimization results.

lower heat transfer coefficients). The analysis on the thermo-mechanical stresses allows for excluding specific designs from a technical standpoint. Configurations which would result in a pressure drop lower than 0.4 bar, would result in high $\Delta\sigma$ and σ_{max} and are, therefore, not ideal.

Figure 12c presents the results for different thermal energy storage sizes. The results suggest that the higher the storage size, the lower the impact of SGS design on the LCOE. This is because the yearly electricity production is increased, and the energy produced during the start-up procedures represent a lower fraction of the total production. This effect increases with decreasing SGS pressure drop. For the lowest pressure drop, the difference in LCOE increase varies by up to 0.5 % among the three different storage sizes. However, the difference in LCOE among the storage sizes decreases as the pressure drop increases. Table 7 presents the performance and geometry data of the optimal SGS design (the one corresponding to the maximum pressure drop on the water side, 1.96 bar). A large number of tube layers and tubes for each layer minimize the pressure drop on the SH, which com-

prises 66 % of the total water pressure drop. The evaporator constitutes the highest cost, comprising 44 % of the steam generator system total cost.

Table 7: Performance and geometry data of the optimal SGS design.

Parameter	Units	ECO	EVA (†)		SH	RHe	RHs
Shell diameter	[mm]	1429	1359	1654	1436	2018	1993
Shell length	[mm]	9.25	10.7	7.68	7.69	10.13	7.71
Shell thickness	[mm]	16	59	77	18	21	23
Number of shells	[-]	1	2	1	1	1	1
Tube outer diameter	[mm]	30	30		30	30	30
Tube thickness	[mm]	3.1	4		3.1	3.1	3.1
Tube layers	[-]	21	20		38	35	37
Tube per layers	[-]	6	3		8	15	15
Tube coils	[-]	39	3		27	7	7
Header diameter	[mm]	191.1	341.5		254.8	550.9	495.2
Header thickness	[mm]	18.0	35.2		24.0	17.0	15.0
Tube side average flow velocity	[m/s]	0.95	3.17		12.02	22.44	22.31
Shell side average flow velocity	[m/s]	1.14	-		1.28	0.55	0.49
Tube side heat transfer coefficient	[W/(m^2 K)]	7781.9	5192.6		3477.8	779.2	632.7
Shell side heat transfer coefficient	[W/(m^2 K)]	2355.9	21964.8		2329.4	1511.6	1301.8
Overall heat transfer coefficient	[W/(m^2 K)]	1514.4	3349.4		1155.2	425.0	352.8
Oil side pressure drop	[bar]	0.435	1.085		0.389	0.046	0.214
Water side pressure drop	[bar]	0.189	0.016		1.331	0.214	0.219
Purchase equipment cost	[mil USD]	0.260	0.597		0.211	0.109	0.177

(†) The shell parameters refer to the heat exchangers (on the left) and steam drum (on the right).

3.3. Transient performance results for the start-up procedure

Figure 13 presents the results of the start-up procedure for the main thermodynamic parameters and mass flow rates both for the water and the HTF. Figures 13a and 13b summarize the results for the water side, considering the superheater (red lines) and reheater (grey lines) pressure and temperature and total steam mass flow rate for one SGS train. Each figure denotes the three start-up procedure phases (1: initiation, 2: roll-up, 3: loading-up phase) with vertical dash dotted lines and the corresponding numbers according to the control logic depicted in Figure 8. The results in this Section are related to the optimal design for the highest pressure drop point (1.96 bar), as presented in Table 7. The average heating rates for the evaporator and superheater were kept at 8.5 K/min and 15 K/min as they represent the minimum value each design solution can reach (see Table 3). The HTF temperature and mass flow rate are controlled to keep the heating rates below or equal to the allowable values.

After 1.4 minutes, the HTF temperature starts to rise according to the allowable superheater heating rates (see Figure 8, phase 1). Once the steam temperature reaches the minimum allowable temperature for the steam turbine, the start-up procedure initiates, and the turbine starts the roll-up and synchronization phase (phase 2). During this phase, the excess of mass flow rate is bypassed. Once this phase is finished, after 8 minutes, the HTF mass flow rate starts to rise (see Figure 13c) and the flow rate slope increases, as the pressure increases due to higher allowable heating rates (phase 3). After 27.6 minutes, the start-up procedure is finished, and the SGS reaches the nominal values. These results are in line with the start-up procedure presented in Ref. [66]. The authors obtained a steam generator start-up procedure lasting for around 33 minutes. The difference between the results in this Section and the ones presented in Ref. [66] is attributed to the assumption of a slower SH in Ref. [66]. This causes phase 1 to last around 10 minutes in the results presented in Ref. [66] as opposed to the 5 minutes obtained in this work. Moreover, lower heating rate constraints (7 K/min) were also used by Gonzalez-Gomez et al. [74], resulting in 15 minutes for phase 1. The comparisons indicate that the use of an optimized SH from the dynamic operation perspective would reduce the SGS start-up procedure by 15.2 % and by 27 % compared to the results of Ref. [66] and Ref. [74], respectively.

Figure 14 illustrates the stress results, which are normalized with respect to the corresponding ultimate tensile strength (UTS). Figure 14 also indicates the start-up phase numbers according to the control logic depicted in Figure 8 with vertical dash dotted lines, while the horizontal dashed lines represent the stress limits according to the norm. Figures

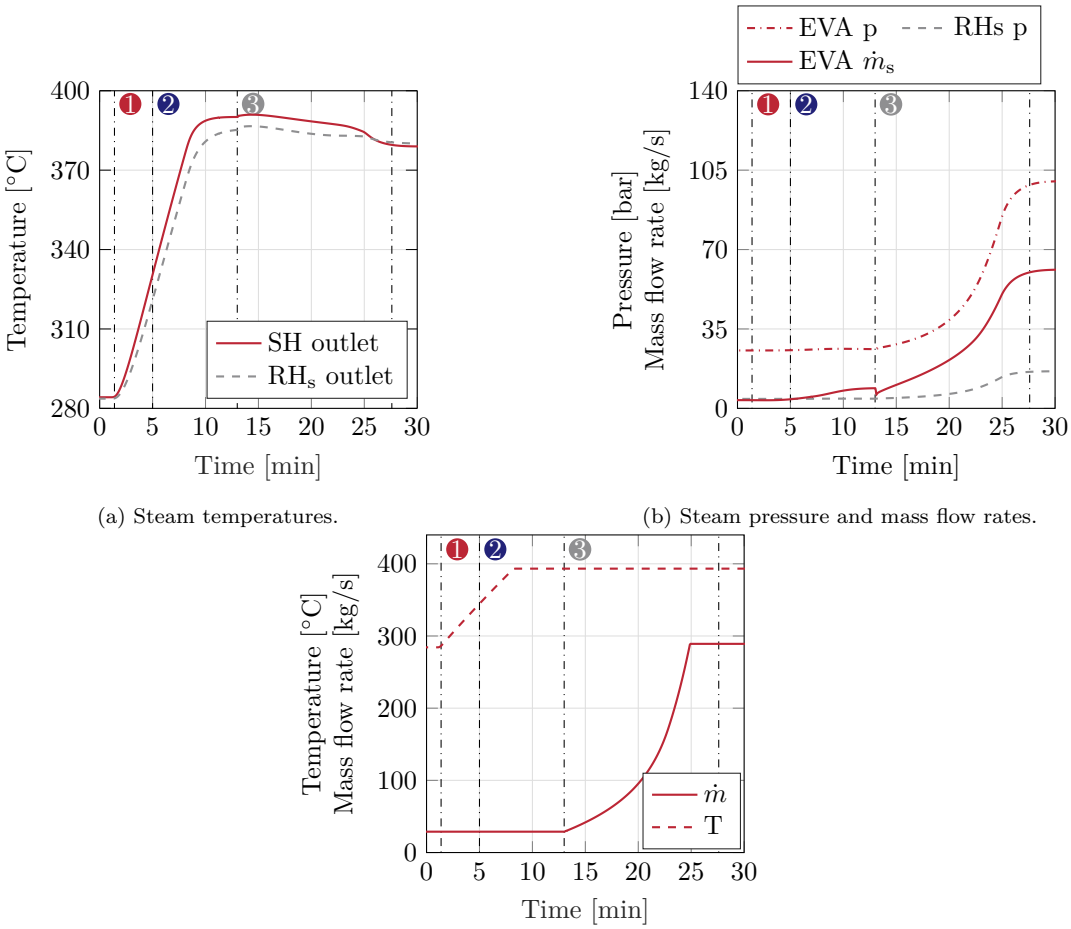

(a) Steam temperatures.

(b) Steam pressure and mass flow rates.

(c) HTF temperature and mass flow rate.

Figure 13: Transient performance results for the start-up procedure of the steam generator.

14a, 14b, and 14c depict the results for the superheater inlet header, outlet header and steam drum junctions, respectively. The results suggest that the inlet header is more exposed to stresses than the other header. This is related to higher temperature differences between the hot and the cold fluid in the inlet header than those of the outlet header. The thermal and pressure stresses of the outlet header are mainly increasing during phases 2 and 3 of the start-up procedure. An increase is observed during phase 1 and at the beginning of phase 2 for the outlet header. The outlet header experiences higher differences between the maximum and minimum values of the total stress. This is explained by the lower temperature difference between the hot and the cold fluid, which implies lower thermal stresses at the beginning of the start-up procedure.

In all cases, the total stress is within the allowable limits as all the components are designed to guarantee a 25-year lifetime according to the EN 12952-3. However, the different

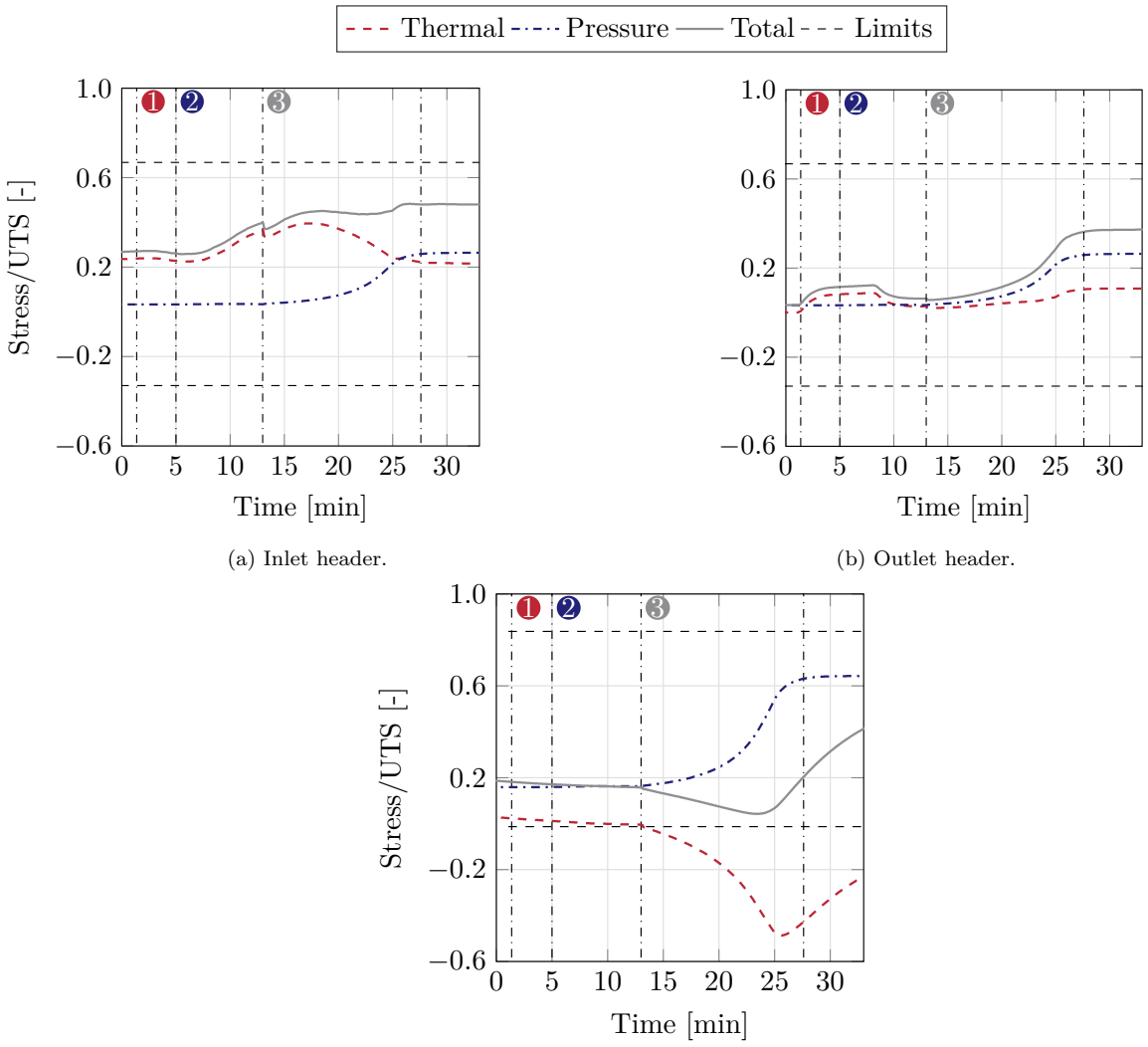

(a) Inlet header.

(b) Outlet header.

(c) Steam drum.

Figure 14: Stress results during the start-up procedure.

optimized designs experience different stress profiles, as the maximum allowable heating rates vary among the design points. Gonzalez-Gomez et al. [74] presented an analysis of the transient stress response during a start-up procedure of the steam generator for parabolic trough power plants. The authors assumed a fixed heating rate constraint and calculated the stress development. However, they obtained stresses exceeding the limits for the superheater components, suggesting that it is essential to include the LCF constraints during the design phase to optimize properly the start-up procedure. In the results presented in Ref. [74], the steam drum experienced stresses within the allowable limits set by the EN 12952-3.

4. Conclusions

This paper presented a novel method to design a header and coil steam generator system accounting for its dynamic performance, stress sensitivity and impact on the power plant techno-economic performance for a parabolic trough power plant with thermal energy storage. A design tool, previously developed by the authors, was integrated with a transient model in order to design and evaluate the dynamic performance of the steam generator systems during start-up procedures. The model included the calculation of thermo-mechanical stresses of the superheater headers and steam drum/downcomer junction.

The outcome of the validation indicates that the dynamic model provides accurate results, with a maximum deviation at steady-state nominal load conditions of 2.8 % for the degree of superheat at the outlet of the superheater. In transient conditions, the feedwater mass flow rate and re-heater steam outlet temperature present the highest normalized root mean square errors, 8.1 % and 7.7 %, respectively, while all the other parameters analyzed present deviations below 7 %. By considering both low-cycle fatigue and transient requirements, the multi-objective optimization results indicate that a 30 mm tube outer diameter is the optimal solution for the case considered, as lower parasitic consumption in case of higher tube diameters would not compensate for the increase in cost and slower dynamic response of the steam generator system. By considering thermal stress sensitivity of the components, the results suggest that high pressure drop solutions are preferred as they minimize the stress difference and maximum stress during the start-up phase. Specifically, the highest water side pressure drop solution (1.96 bar) is chosen as the optimal point as it presents the lowest levelized cost of electricity. The sensitivity study on the thermal energy storage size indicates that for larger storage sizes, the impact on the power plant levelized cost of electricity tends to increase; however, this difference tends toward zero if high pressure drop solutions are chosen. For the optimal design, the duration of the steam generator system start-up procedure is 27.6 minutes, while the thermo-mechanical stresses are within the limits governed by the norms for all components. The inlet superheater header experiences higher thermal stresses than its outlet counterpart, while the steam drum experiences the highest total stress and stress differences during the start-up procedure.

References

[1] International Energy Agency. Technology Roadmap, Solar Thermal Electricity. Technical report, IEA, Paris, France, 2014.

[2] R. Domínguez, M. Carrión, and G. Oggioni. Planning and operating a renewable-dominated european power system under uncertainty. *Applied Energy*, 258:113989, 2020.

[3] T. R. Mancini, J. A. Gary, G. J. Kolb, and C. Ho. Power Tower Technology Roadmap and cost reduction plan. Sandia Report. Technical Report Sandia Report, April, Sandia, Sandia National Laboratories. Albuquerque, New Mexico, 2011.

[4] World Energy Council. World Energy Resources: Solar 2016. Technical report, London, England, 2016.

[5] Groupe Reaction Inc. CSP Parabolic Trough Report : Cost , Performance and Key Trends. Technical report, CSP Today, London, England, 2014.

[6] Estela, Greenpeace, and Solarpaces. Solar Thermal Electricity - Global Outlook 2016. Technical report, Brussels, Belgium, 2016.

[7] Antonio Colmenar-Santos, Elisabet Palomo-Torrejón, Francisco Mur-Pérez, and Enrique Rosales-Asensio. Thermal desalination potential with parabolic trough collectors and geothermal energy in the spanish southeast. *Applied Energy*, 262:114433, 2020.

[8] D. Ferruzza, M. Topel, B. Laumert, and F. Haglind. Impact of steam generator start-up limitations on the performance of a parabolic trough solar power plant. *Solar Energy*, 169:255–263, 2018.

[9] P. Dzierwa and J. Taler. Optimum Heating of Pressure Vessels With Holes. *Journal of Pressure Vessel Technology*, 137(1):011202, 2014.

[10] P. Dzierwa, D. Taler, M. Trojan, and J. Taler. Evaporator Heating with Optimum Fluid Temperature Changes. *Procedia Engineering*, 157:29–37, 2016.

[11] J. Taler, B. Weglowski, D. Taler, T. Sobota, P. Dzierwa, M. Trojan, P. Madejski, and M. Pilarczyk. Determination of start-up curves for a boiler with natural circulation based on the analysis of stress distribution in critical pressure components. *Energy*, 92:153–159, 2015.

[12] CEN. Water-tube boilers and auxiliary installations - Part 3: Design and calculation for pressure parts of the boiler. Technical report, European Committee for Standardization, Brussels, Belgium, 2012.

[13] M. Topel, Å. Nilsson, M. Jöcker, and B. Laumert. Investigation Into the Thermal Limitations of Steam Turbines During Start-Up Operation. *Journal of Engineering for Gas Turbines and Power*, 140(1):012603, 2017.

[14] M. Topel, R. Guédez, and B. Laumert. Impact of Increasing Steam Turbine Flexibility on the Annual Performance of a Direct Steam Generation Tower Power Plant. *Energy Procedia*, 69(0):1171–1180, 2015.

[15] L. L. Vant-Hull. *Central tower concentrating solar power (CSP) systems*. Woodhead Publishing Limited, Houston, Texas, 2012.

[16] P.A. González-Gómez, F. Petrakopoulou, J.V. Briongos, and D. Santana. Cost-based design optimization of the heat exchangers in a parabolic trough power plant. *Energy*, 123:314–325, 2017.

[17] L. Pelagotti, K. Sørensen, T. Condra, T. Joseph, and A. Franco. Modelling of a Coil Steam Generator for CSP applications. In *Proceedings of the 55th International Conference on Simulation and Modelling*, 2014.

[18] D. Ferruzza, M. R. Kærn, and F. Haglind. Design of header and coil steam generator for concentrating

solar power applications accounting for low-cycle fatigue requirements. *Applied Energy*, 236(2019):793–803, 2018.

[19] Aalborg CSP. http://www.aalborgcsp.com/quickmenu/brochures/. [accessed: 2017-08-03].

[20] L. Chen, C. Yan, and J. Wang. Multi-objective optimal design of vertical natural circulation steam generator. *Progress in Nuclear Energy*, 68:79 – 88, 2013.

[21] C. Liu, C. Yan, and J. Wang. Optimal design of vertical natural circulation steam generator. *Nuclear Engineering and Design*, 252:167 – 178, 2012.

[22] S. Mercati, M. Milani, L. Montorsi, and F. Paltrinieri. Design of the steam generator in an energy conversion system based on the aluminum combustion with water. *Applied Energy*, 97:686 – 694, 2012. Energy Solutions for a Sustainable World - Proceedings of the Third International Conference on Applied Energy, May 16-18, 2011 - Perugia, Italy.

[23] J. Gómez-Hernández, P.A. González-Gómez, J.V. Briongos, and D. Santana. Influence of the steam generator on the exergetic and exergoeconomic analysis of solar tower plants. *Energy*, 145:313 – 328, 2018.

[24] M. Lin, J. Reinhold, N. Monnerie, and S. Haussener. Modeling and design guidelines for direct steam generation solar receivers. *Applied Energy*, 216:761 – 776, 2018.

[25] Soteris A Kalogirou, Constantinos C Neocleous, and Christos N Schizas. Artificial neural networks for modelling the starting-up of a solar steam-generator. *Applied Energy*, 60(2):89 – 100, 1998.

[26] M. Serna and A. Jiménez. A compact formulation of the Bell-Delaware method for heat exchanger design and optimization. *Chemical Engineering Research and Design*, 83(5 A):539–550, 2005.

[27] Robert W. Serth and Thomas G. Lestina. *The Stream Analysis Method*. Academic Press, Boston, Massachusetts, second edition edition, 2014.

[28] D. Q. Kern. *Process Heat Transfer*. McGraw-Hill, Singapore, 1965.

[29] D. Anarratore. *Steam generators. Description and design.* Springer, Milano, Italy, 2008.

[30] D. Anarratore. *Handbook for heat exchangers and tube banks design.* Springer, Milano, Italy, 2010.

[31] G. P. Purohit. Estimating costs of shell-and-tube heat exchangers. *Chemical Engineering*, (90):56–67, 1983.

[32] M^{a}. D. Durán, M. Valdés, A. Rovira, and E. Rincón. A methodology for the geometric design of heat recovery steam generators applying genetic algorithms. *Applied Thermal Engineering*, 52(1):77–83, 2013.

[33] Alessandro F. and N. Giannini. A general method for the optimum design of heat recovery steam generators. *Energy*, 31(15):3342–3361, 2006.

[34] P. Wildi-Tremblay and L. Gosselin. Minimizing shell-and-tube heat exchanger cost with genetic algorithms and considering maintenance. *International journal of energy research*, 31(31):135–147, 2007.

[35] P.A. González-Gómez, J. Gómez-Hernández, D. Ferruzza, F. Haglind, and D. Santana. Dynamic performance and stress analysis of the steam generator of parabolic trough solar power plants. *Applied Thermal Engineering*, 147:804 – 818, 2019.

[36] P.A. González-Gómez, J. Gómez-Hernández, J.V. Briongos, and D. Santana. Transient thermo-mechanical analysis of steam generators for solar tower plants. *Applied Energy*, 212:1051 – 1068, 2018.

[37] N. Mertens, F. Alobaid, R. Starkloff, B. Epple, and H. Kim. Comparative investigation of drum-type

and once-through heat recovery steam generator during start-up. *Applied Energy*, 144:250 – 260, 2015.

[38] P.A. González-Gómez, J. Gómez-Hernández, J.V. Briongos, and D. Santana. Lifetime analysis of the steam generator of a solar tower plant. *Applied Thermal Engineering*, 159:113805, 2019.

[39] P. A. González-Gómez, F. Petrakopoulou, Javier V. Briongos, and D. Santana. Steam generator design for solar towers using solar salt as heat transfer fluid. In *AIP Conference Proceedings*, volume 1850, 0300, pages 1–8, 2017.

[40] Rafael Guedez, Monika Topel, Francisco Ferragut, Irene Callaba, and Carlos David Perez-segarra. A Methodology for Determining Optimum Solar Tower Plant Configurations and Operating Strategies to Maximize Profits Based on Hourly Electricity Market Prices and Tariffs. *Solar Energy Engineering*, 138(April 2016):1–12, 2017.

[41] D. Ferruzza, M. Topel, I. Basaran, B. Laumert, and F. Haglind. Start-Up Performance of Parabolic Trough Concentrating Solar Power Plants. In *AIP Conference Proceedings 1850*, volume 1850, 1600, pages 1–9, 2017.

[42] MATLAB. *version 9.1.0.4 (R2016b)*. The MathWorks Inc., Natick, Massachusetts, 2016.

[43] University of Wisconsin Madison. Solar Energy Laboratory. TRNSYS, a transient simulation program. Technical report, 1975.

[44] DLR. A TRNSYS Model Library for Solar Thermal Electric Components (STEC). Technical Report November, 2006.

[45] D. Cooke. Modeling of off-design multistage turbine pressures by stodola's ellipse. In *Energy Incorporated PEPSE User's Group Meeting, Richmond, VA, Nov*, pages 2–3, 1983.

[46] V. Dudley. SEGS LS-2 Solar Collector. Test Results. Technical report, Sandia National Laboratories. Albuquerque, New Mexico, 1994.

[47] P Gilman, National Renewable Energy Laboratory, and Sandia National Laboratories. Solar advisor model user guide for version 2.0. Technical Report August, National Renewable Energy Laboratory, (NREL), Cole Boulevard, Colorado, 2008.

[48] F. Lippke. Simulation of the Part-Load Behavior of a 30 Mwe SEGS Plant. Report. Technical report, Sandia National Laboratories. Albuquerque, New Mexico, 1995.

[49] G. Leyland and D. Favrat. *Multi-objective optimization applied to industrial energy problems*. PhD thesis, École Polytechnique Féderale de Lausanne, (EPFL), Lausanne, 2002.

[50] M. Dempsey. Dymola for multi-engineering modelling and simulation. In *2006 IEEE Vehicle Power and Propulsion Conference*, pages 1–6, Sept 2006.

[51] R.K. SINNOTT. Chapter 12 - heat-transfer equipment. In R.K. Sinnot, editor, *Coulson and Richardson's Chemical Engineering*, Chemical Engineering Technical Series, pages 565 – 702. Pergamon, Amsterdam, second edition, 1993.

[52] C. Merritt. *Process Steam Systems: A Practical Guide for Operators, Maintainers, and Designers*. John Wiley & Sons, New Jersey, 2015.

[53] American society of mechanical engineers. *ASME Boiler and Pressure Vessel Code: Section VIII - Division 2*. New York, New York, 2015.

[54] F. Casella and A. Leva. Object-oriented modelling amp;amp;amp; simulation of power plants with modelica. In *Proceedings of the 44th IEEE Conference on Decision and Control*, pages 7597–7602, Dec 2005.

[55] J. Bonilla, L.J. Yebra, and S. Dormido. Chattering in dynamic mathematical two-phase flow models. *Applied Mathematical Modelling*, 36(5):2067 – 2081, 2012.

[56] J Bonilla, LJ Yebra, and S Dormido. Mean densities in dynamic mathematical two-phase flow models. *Computer Modeling in Engineering and Sciences (CMES)*, 67(1):13, 2010.

[57] S. Patankar. *Numerical heat transfer and fluid flow*. Series on Computational Methods in Mechanics and Thermal Science. Hemisphere Publishing Corporation (CRC Press, Taylor & Francis Group), 1980.

[58] L. R. Petzold. A description of DASSL: a differential/algebraic system solver. In *Scientific computing (Montreal, Quebec, 1982)*, pages 65–68. IMACS, New Brunswick, NJ, 1983.

[59] S.G. Kandlikar. Heat transfer characteristics in partial boiling, fully developed boiling and significant void flow regions of subcooled flow boiling. *Journal of Heat Transfer*, 120:395–401, 1998.

[60] D. R. Nørhave. Development of a dynamic model for a steam generator for concentrated solar power applications. bachelor thesis, 2017.

[61] A Benato, Martin Ryhl Kærn, Leonardo Pierobon, A Stoppato, and Fredrik Haglind. Analysis of hot spots in boilers of organic rankine cycle units during transient operation. *Applied Energy*, 151:119–131, 2015.

[62] K. J. Åström and R. D. Bell. Drum-boiler dynamics. *Automatica*, 36(3):363–378, 2000.

[63] S. W. Churchill and H. S. Chu. Correlating equations for laminar and turbulent free convection from a horizontal cylinder. *International journal of heat and mass transfer*, 18(9):1049–1053, 1975.

[64] V. Ganapathy. Understanding boiler circulation. *Chemical Engineering*, 120(10):52–56, 2013.

[65] M. Topel and B. Laumert. Improving concentrating solar power plant performance by increasing steam turbine flexibility at start-up. *Solar Energy*, 165:10 – 18, 2018.

[66] H. Schenk, J. Dersch, T. Hirsch, and T. Polklas. Transient simulation of the power block in a parabolic trough power plant. In *Proceedings of the 11th International Modelica Conference, Versailles, France, September 21-23, 2015*, number 118, pages 605–614. Linköping University Electronic Press, 2015.

[67] J. G. Ziegler and N. B. Nichols. Optimum settings for automatic controllers. *Trans. ASME*, 64(11), 1942.

[68] R. Skeel and M. Berzins. A method for the spatial discretization of parabolic equations in one space variable. *SIAM Journal on Scientific and Statistical Computing*, 11(1):1–32, 1990.

[69] T. Bergman, A. Lavine, F. Incropera, and D. Dewitt. *Fundamentals of heat and mass transfer*. John Wiley and sons, Jefferson city, Missouri, 7th edition, 2011.

[70] T. S. Kim, D. K. Lee, and S. T. Ro. Analysis of thermal stress evolution in the steam drum during start-up of a heat recovery steam generator. *Applied Thermal Engineering*, 20(11):977–992, 2000.

[71] S. K. Chakrabory, N. Manna, and S. Dey. Importance of tree-elements boiler drum level control its installation in power plant. *International Journal of Instrumentation and Control Systems*, 4(2):1–12, 2014.

[72] Y. Murakami and K.J. Miller. What is fatigue damage? a view point from the observation of low cycle fatigue process. *International Journal of Fatigue*, 27(8):991 – 1005, 2005. Cumulative Fatigue Damage Conference - University of Seville 2003.

[73] Solar Millennium AG. The parabolic trough power plants andasol 1 to 3. Technical report, Erlangen, Germany, 2008.

[74] P.A. González-Gómez, J. Gómez-Hernández, D. Ferruzza, F. Haglind, and D. Santana. Dynamic

performance and stress analysis of the steam generator of parabolic trough solar power plants. *Applied Thermal Engineering*, 147:804 – 818, 2019.